Integrated Assessment **2:** 183–197, 2001.

Climate impact response functions for terrestrial ecosystems

Hans-Martin Füssel [a,*] and Jelle G. van Minnen [b]

[a] *Potsdam Institute for Climate Impact Research, Telegrafenberg, 14473 Potsdam, Germany*
E-mail: fuessel@pik-potsdam.de
[b] *National Institute of Public Health and the Environment, Department for Environmental Assessment, Box 1, 3720 BA Bilthoven, The Netherlands*
E-mail: jelle.van.minnen@rivm.nl

Received 22 November 1999; revised 30 March 2001

We introduce climate impact response functions as a means for summarizing and visualizing the responses of climate-sensitive sectors to changes in fundamental drivers of global climate change. In an inverse application, they allow the translation of thresholds for climate change impacts ('impact guard-rails') into constraints for climate and atmospheric composition parameters ('climate windows'). It thus becomes feasible to specify long-term objectives for climate protection with respect to the impacts of climate change instead of crude proxy variables, like the change in global mean temperature. We apply the method to assess impacts on terrestrial ecosystems, using the threat to protected areas as the central impact indicator. Future climate states are characterized by geographically and seasonally explicit climate change patterns for temperature, precipitation and cloud cover, and by their atmospheric CO_2 concentration. The patterns are based on the results of coupled general circulation models. We study the sensitivity of the impact indicators and the corresponding climate windows to the spatial coverage of the analysis and to different climate change projections. This enables us to identify the most sensitive biomes and regions, and to determine those factors which significantly influence the results of the impact assessment. Based on the analysis, we conclude that climate impact response functions are a valuable means for the representation of climate change impacts across a wide range of plausible futures. They are particularly useful in integrated assessment models of climate change based on optimizing or inverse approaches where the on-line simulation of climate impacts by sophisticated impact models is infeasible due to their high computational demand.

Keywords: climate impact response functions, terrestrial ecosystems, protected areas, global climate change, integrated assessment model, ICLIPS model, guard-rail approach, SRES scenarios

1. Introduction

Through a wide range of activities, humankind is altering the composition of the atmosphere and changing the climate on Earth [1]. There is increasing evidence that recent climatic change has altered the range, the physiology, and the seasonal cycle of plants [2–5] and animals [6–8], and that it already led to the extinction of species [9]. Major and abrupt climatic changes have often had devastating effects on biodiversity in prehistorical times. About 200 million years ago, for instance, the end-Triassic mass extinction event resulted in more than 95% turnover of megafloral species. A three- to fourfold increase in CO_2 (due to extensive basaltic volcanicity) associated with a 3–4°C rise in global mean temperature has been suggested as the basic cause for this event [10].

The impact of anticipated climate change on natural vegetation has been extensively studied over the last years. Major themes of interest were the equilibrium vegetation distribution in a changed climate [11–14], the transient response of ecosystems to climate change [15–17], and the feedback of vegetation change on the biogeochemical cycles [18–23].

Contrary to existing studies that assess the vegetation response to climate change for specific scenarios only, we present simulated impacts for a wide range of plausible futures in the form of *climate impact response functions* (CIRFs). On the one hand, CIRFs enable the identification of sensitive regions and key drivers for vegetation change. On the other hand, CIRFs allow to translate guard-rails for vegetation impacts backwards into corresponding climate windows, i.e., subsets of their domain.

The CIRFs presented in this paper form a part of the ICLIPS (**I**ntegrated Assessment of **Cli**mate **P**rotection **S**trategies) model. This integrated assessment model of climate change is based on the guard-rail approach (syn. tolerable windows approach), a novel decision-analytical framework for the integrated modelling of climate change [24].

Policy-makers involved in the implementation of the United Nations Framework Convention on Climate Change (UNFCCC) are faced with its ambitious objective stated in Article 2 "to prevent dangerous anthropogenic interference with the climate system" and, at the same time, "to enable economic development to proceed in a sustainable manner" [25]. A typical application of the ICLIPS model starts from normatively specified impact guard-rails and additional socio-economic constraints that shall make these potentially conflicting goals manageable. In a second step, sets of 'tolerable' climate protection strategies are determined numerically by simultaneously obeying all constraints [26–28].

* Corresponding author.

Since the final specification of 'appropriate' guard-rails is made by policy-makers, not by scientists, the guard-rail approach allows for a clear separation of the inherently normative decision on minimum requirements for climate policy on the one hand, and the scientific analysis of the relevant parts of the Earth system on the other hand.

This paper is organized as follows. In section 2, we describe the methods and models applied. Model results, including various sensitivity tests, are presented in section 3, and section 4 concludes the paper.

2. Methods

In this section, we present the underlying models and methods for the assessment of climate impacts on natural vegetation. We start with a description of the vegetation model and of the chosen impact indicators. Subsequently, we explain the climate projections applied and introduce the concept of climate impact response functions. We close with a presentation of various sensitivity analyses.

2.1. Modelling of vegetation impacts

We apply the equilibrium vegetation model BIOME 1 [29], adapted for IMAGE 2.1 [30,31], to simulate the vegetation distribution for current and future climate states on a 0.5° latitude by 0.5° longitude grid. The model determines the potential vegetation in a grid cell based on monthly data for temperature, precipitation, and solar radiation as well as atmospheric CO_2 and soil properties. In a first step, various bioclimatic indices are derived, for instance the effective temperature sum above certain temperature thresholds and a moisture index. BIOME 1 defines climatic envelopes based on these indices for 16 plant functional types (PFTs). Climatic threshold values for ecosystems are actually observable in nature [32]. These constraints are used in a second step to determine which of the 16 PFTs can principally occur, based on the non-violation of any of the constraints. In a final step, BIOME 1 applies a dominance hierarchy as a proxy for competition between different PFTs. 14 biomes are defined as combinations of one or more PFTs at the same hierarchy level. For a list of all biomes, see figure 4.

BIOME 1 has been extensively used for assessing the response of natural vegetation to anticipated climatic changes [33,34]. Improvements in IMAGE 2.1 include the effects of elevated CO_2 levels on the water-use efficiency of plants. Indirect impacts of climate change on vegetation due to altered disturbance regimes (e.g., forest fires, insect pests, and wind storms) and transient processes such as migration are not considered in the model.

Progress has recently been achieved in developing *dynamic* vegetation models [35–37]. The level of physiological detail included in these models allows to simulate short-term vegetation change, and to assess the productivity and the carbon dynamics of ecosystems. Dynamic aspects were shown, however, to be of minor importance for indicators that are solely based on the long-term distribution of biomes [16]. The application of a structurally simpler and computationally more efficient biome model is therefore justified in the ICLIPS model.

2.2. Aggregated indicators for vegetation impacts

Similar to previous studies of this subject [11,14,38], we use the percentage of an area where the current biome is no longer viable as the *main* indicator to quantify the impacts of climate change on natural vegetation. This indicator values all simulated biome changes equal. We have intentionally refrained from applying more elaborated distance measures between biomes, like the "dissimilarity index" [39], because we suspect them to be less comprehensible for the non-expert users of the ICLIPS model. Since biomes are rather coarse categories, significant ecosystem impacts may occur even if no biome change is simulated. In areas with high biodiversity, for instance in most tropical forests, species generally have a small niche volume and are thus particularly sensitive to climatic change [40,41]. The figures presented in this paper are therefore regarded as low estimates of climate impacts on ecosystems.

There are various ways for "ecosystems to adapt naturally to climate change" (UNFCCC, Art. 2), namely by acclimatization, migration, and evolution. Evolution typically occurs at time scales that are much longer than those associated with anthropogenic climate change. Migration is therefore the most important adaptation mechanism for ecosystems beyond their limits of physiological acclimatization. It represents, however, only an inferior adaptation since ecosystems will not move wholesale in response to climate change.

We will generally restrict the analysis of vegetation impacts to protected areas like nature reserves, national parks, and wildlife sanctuaries. Migration has only limited relevance for areas that are legally protected in their *current* state. Any major vegetation change will typically threaten the very objectives for their protection, no matter whether it occurs fast or slow. Furthermore, other anthropogenic stress factors like land-use change are generally less important in protected areas than elsewhere.

From an ecological point of view, it might appear desirable to assign higher weights to impacts in species-rich areas and centers of endemism than elsewhere [42,43]. However, we do not implement this idea since such an attempt to increase the 'scientific power' of the aggregated impact indicator is likely to decrease its comprehensibility to non-experts.

As *additional* impact indicators, we use the stable area and the total area of individual biomes relative to the baseline figure, whereby the entire land area is considered. The stable area corresponds to a pessimistic view of adaptation that does not account for the establishment of biomes at locations that become climatically suitable in the future. The total area corresponds to a rather optimistic view where biomes suddenly pop up as soon as the climatic conditions become suitable, regardless of restrictions related to dispersion potentials and the availability of migration corridors. While

the stable area never exceeds the baseline area, the total area can be either smaller or larger.

2.3. Climate projections

Computational restrictions require integrated assessment models to apply reduced-form substitutes of complex climate models. Various approaches have been developed to construct climate change scenarios for (global) impact analyses. Two of them are particularly suitable for the parameterized description of a wide range of future climate states [44–47].

In the *incremental changes approach*, changes in a few climate variables (typically annual temperature and precipitation) are applied uniformly across the entire region under consideration [48]. While this approach is useful for a general assessment of potential climate change impacts, it does not take advantage of the information available from complex climate models.

The *scaled scenario approach* describes future climate change by scaling spatial patterns of climate anomalies to the respective change in the globally and annually averaged near-surface temperature (global mean temperature, GMT). The patterns are derived from forcing experiments with general circulation models (GCMs) and consistently take into account the spatial and seasonal variability of the simulated climate anomalies. The scaled scenario approach is based on the assumption that the transient change in many pertinent climate variables is approximately linearly dependent on the change in GMT. Additional dimensions would be required to capture important non-linear effects, for instance, a regional cooling caused by a weakening of the global ocean circulation [49].

The ICLIPS climate model implements the scaled scenario approach. Efficiency and flexibility are achieved by approximating the results of transient GCM experiments under increasing greenhouse gas concentrations through a separate description of their dynamical behaviour and their spatial variability. The following characteristics of transient GCM experiments are mimicked by the ICLIPS climate model.

1. The **climate sensitivity** of a climate model, denoted as $\Delta T_{2\times CO_2}$, is defined as the *equilibrium* change in GMT following a doubling of the equivalent CO_2 concentration. The latter states the concentration level of CO_2 that yields the same radiative forcing as the combination of all greenhouse gases in the atmosphere. Since sufficiently long integrations of fully coupled GCMs would be too costly, their climate sensitivity needs to be approximated. This is most commonly achieved by coupling the atmospheric GCM component to a simple mixed-layer ocean. Alternatively, a technique based upon a linear response theory can be applied (see equation (4)). Estimates of $\Delta T_{2\times CO_2}$ for a GCM may vary depending on the applied approximation technique and the specific integration that they are based on.

2. The **temporal response** of a GCM to an increasing forcing can be approximately described by a linear impulse response function (IRF) of the form

$$\Delta T(t) \equiv \int_{t_0}^{t} \Delta Q(u) \cdot R(t-u)\,\mathrm{d}u, \tag{1}$$

$$\Delta Q(t) \equiv \log_2 \frac{C(t)}{C(t_0)}. \tag{2}$$

$\Delta T(t)$, $\Delta Q(t)$ and $C(t)$ are the time paths of the change in GMT, the normalized change in radiative forcing (both compared to the base year t_0), and the *equivalent* CO_2 concentration, respectively. The *Green function* $R(t)$ can be represented as superposition

$$R(t) \equiv \sum_{i=1}^{n} A_i \cdot \frac{\mathrm{e}^{-t/\tau_i}}{\tau_i} \tag{3}$$

of a number of exponentials of different amplitudes A_i and (real) relaxation times τ_i [50]. These parameters are obtained by fitting the IRF to the results of a transient GCM experiment.

Equation (1) assumes a linear relationship between radiative forcing and *equilibrium* GMT changes. This is a quite common presumption although it is only approximately correct due to various nonlinear processes, for instance, the ice-albedo feedback [51].

Integration of equation (1) for an instantaneous CO_2 doubling, i.e.,

$$\Delta Q(t) \equiv \begin{cases} 0, & t \leqslant t_0, \\ 1, & t > t_0, \end{cases}$$

leads to the following characterization of the *climate sensitivity*

$$\begin{aligned} \Delta T_{2\times CO_2} &\equiv \lim_{t\to\infty} \Delta T(t) \\ &= \lim_{t\to\infty} \left(\sum_{i=1}^{n} A_i \cdot \left(1 - \mathrm{e}^{-(t-t_0)/\tau_i}\right) \right) \\ &= \sum_{i=1}^{n} A_i. \end{aligned} \tag{4}$$

The relaxation time of the slowest exponential is typically of the same magnitude or even longer than the length of a GCM integration. Estimates of its amplitude and eventually of the climate sensitivity are therefore subject to some uncertainty [52].

In order to describe the temporal response of a GCM independent of its climate sensitivity, the Green function can be normalized by defining

$$\tilde{R}(t) \equiv \sum_{i=1}^{n} \tilde{A}_i \cdot \frac{\mathrm{e}^{-t/\tau_i}}{\tau_i}, \tag{5}$$

$$\tilde{A}_i \equiv \frac{A_i}{\Delta T_{2\times CO_2}}. \tag{6}$$

The $\tilde{A}_i$, summing up to 1, represent the *fractional* contribution of each exponential to the overall temperature

change. We define the *normalized* change in GMT over time as

$$\Delta\tilde{T}(t) \equiv \frac{\Delta T(t)}{\Delta T_{2\times CO_2}} = \int_{t_0}^{t} \Delta Q(u) \cdot \tilde{R}(t-u)\,\mathrm{d}u. \quad (7)$$

For any greenhouse-gas *stabilization* scenario, it follows that

$$\lim_{t\to\infty} \Delta\tilde{T}(t) = \lim_{t\to\infty} \Delta Q(t) = \lim_{t\to\infty} \log_2 \frac{C(t)}{C(t_0)}. \quad (8)$$

The normalized change in GMT is thus closely linked to the concept of "stabilization of greenhouse gas concentrations in the atmosphere" (UNFCCC, Art. 2). Such a GCM-independent correspondence does not exist for the absolute GMT change.

3. **Climate change patterns** state the change in a climate variable at each location given a unit change in GMT. The most consistent method to separate the spatial and the temporal variability of the climate change signal in a transient GCM experiment under increasing radiative forcing is EOF analysis [53]. The first EOF can be identified with the dominating spatial pattern of anomalies in a climate variable between the scenario and the control run. Alternatively, climate differentials between matching time slices of the control integration and the scenario integration can be used as climate change patterns.

The results from transient climate change experiments performed with warm-start coupled atmosphere–ocean general circulation models provide the best data available for investigating the effects of increasing greenhouse gas concentrations on the global climate system. Even simulations for identical greenhouse gas scenarios differ between GCMs and within members of an ensemble performed with the same GCM [1]. To account for this uncertainty, we use the results of three different GCMs in our modelling exercise.

Evaluating the sensitivity of climate change impacts to the results of different GCM experiments in an integrated assessment model involves the variation of one, two or all three of the characteristics listed above. In many impact assessments, the climate sensitivity is varied across the range from 1.5 to 4.5 K that is considered plausible by IPCC [54], generally without relating it to specific GCM experiments. The effects of varying temporal responses have not received much attention so far, partly because they can only be comprehensively assessed by means of dynamic climate impact models that are still at an early stage of development. Different spatial patterns of climate change are often taken into account in the application of geographically explicit impact models.

The default climate change projection in our analysis is based on two integrations over 850 years of the periodically–synchronously coupled GCM ECHAM3-LSG at T21 resolution (approximately 5.6° by 5.6°) [51,55]. The *equivalent* CO_2 concentration is constantly 345 ppmv (about present-day level) in the control run. In the scenario run, the concentration increases fourfold over a period of 120 years and remains static for the remainder of the simulation. The main reason for the selection of this GCM experiment was its long integration period which made it possible to calibrate a reduced-form climate model to its output [52]. Vegetation–climate feedbacks and the regional climate effects of sulphate aerosols were not considered. Since projections of future SO_2 emissions were significantly reduced by the Intergovernmental Panel on Climate Change (IPCC), the regional climate effects associated with them are expected to be significant only in the early decades of the 21st century [56]. In addition to the ECHAM3 data, we use climate change projections from two alternative GCM experiments that are available through the IPCC Data Distribution Centre. We chose the ECHAM4GGA1 experiment, performed with ECHAM4-OPYC3 at T42 resolution (approximately 2.8° by 2.8°) [57,58] and the HadCM2GGAX ensemble experiment, performed with HadCM2 at a resolution of 2.5° latitude by 3.75° longitude [59].

The normalized IRF (equations (5)–(7)) was calibrated to the output of the multi-century CO_2 quadrupling experiment with ECHAM3 [52]. The resulting estimates for the temporal response are used for all GCM emulations:

$$\tilde{A}_1 = 0.71, \quad \tau_1 = 14\ \mathrm{a},$$
$$\tilde{A}_2 = 0.29, \quad \tau_2 = 450\ \mathrm{a}.$$

Reported figures for the climate sensitivity of a GCM may have been determined by different methods. We thus estimated this parameter based on the available data. The climate sensitivity of ECHAM3 was determined by fitting the IRF model to the results of a transient CO_2 doubling experiment performed with this GCM [51]. Since the ECHAM4 and HadCM2 integrations are based on different forcing scenarios, we calculated the climate sensitivity of those models by dividing the *absolute* GMT change realized in the final 30 year period of the respective integration by the *normalized* GMT change for the same period. The latter was computed by applying equation (7) to the respective forcing scenario. The results, which correspond well with those reported elsewhere, are given in table 1.

The climate change patterns for the ECHAM3 experiment were derived by EOF analysis. The appropriate first EOFs explain 97, 93, and 89% of the variance in the simulated *regional* anomalies for annually, seasonally, and monthly averaged temperature throughout the ECHAM3 simulation, respectively. These figures indicate that the scaled scenario approach provides a good approximation of the climate change signal from the transient GCM experiment. The spatial patterns for the other GCM experiments had to be calculated from the climate differentials between the final 30 year periods of the control integration and the scenario integration because the complete model output required for an EOF analysis was not available.

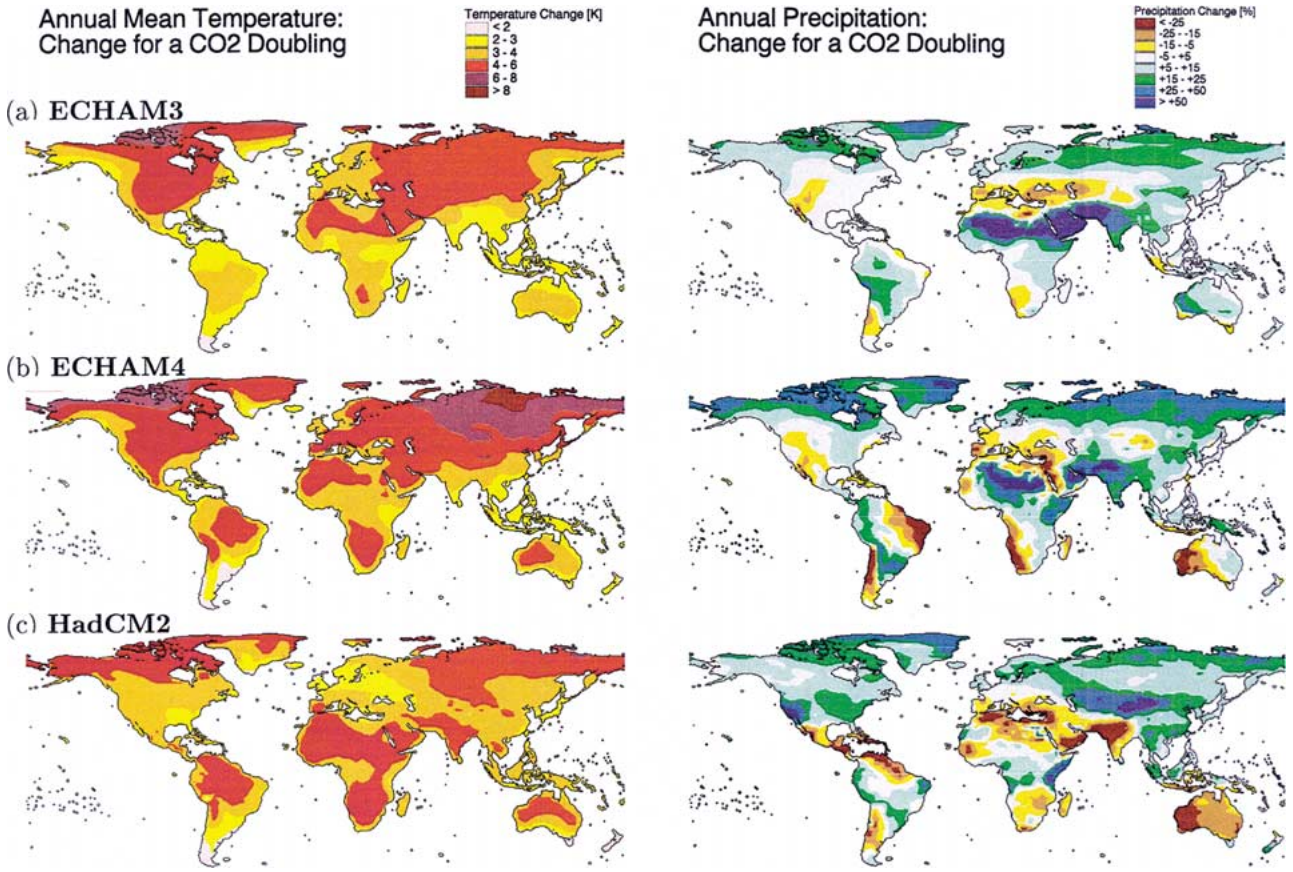

Figure 1. Climate change patterns depicting the changes in annual mean temperature and precipitation as simulated by three GCMs for the stabilized climate after a doubling of the equivalent CO_2 concentration. (a) ECHAM3, (b) ECHAM4, and (c) HadCM2.

We use the 1961–1990 mean climatology developed at the University of East Anglia as the baseline climatology [60]. Due to their huge data and/or computing demands, the application of advanced downscaling techniques like empirical–statistical models or nested climate models is presently not feasible on the global scale [61,62]. Instead, we applied inverse-distance interpolation to map the GCM results onto the finer grid of the baseline climatology [63]. Figure 1 presents the climate change patterns for annual temperature and precipitation. Simulated temperature anomalies are specified in absolute terms whereas changes in precipitation and cloud cover are expressed proportional to the baseline value [64].

2.4. Climate impact response functions

The aim of our inverse impact analysis is to translate constraints from the domain of climate change impacts into the domain of climate variables (in a broad sense). It is, however, not feasible to check for *all* possible climate states whether they comply with a specific impact guardrail. We rather have to characterize plausible future climate states by a few scalar variables that can be scanned efficiently. A CIRF is defined as the dose–effect relationship between such fundamental drivers of global (climate) change on the one hand and a suitable impact indicator on the other hand. The development of CIRFs was inspired by an earlier attempt to develop "ecological response functions" [65]. "Climate-response functions" have also been computed by means of the global impact model (GIM). This model estimates monetized impacts on various economic sectors based upon annual average values for temperature and precipitation at the country level [66].

The first input factor to the CIRFs presented here is the (normalized) change in GMT. The description of future climate states by a single scalar variable leaves freedom for the inclusion of other parameters, like the rate of climate change, measures of climate variability, or socio-economic parameters. For the CIRFs on vegetation impacts, CO_2 concentration is used as the second input factor because of its great relevance for the physiology of plants [67]. Although increasing CO_2 is the principal cause of global climate change, the relationship between CO_2 concentration and transient changes in normalized GMT is not one-to-one due to the thermal lag of the climate system and the influence of non-CO_2 greenhouse gases.

The relationship between the input factors and an impact indicator can be denoted as

$$I = \mathrm{f}_{\mathbf{p}}(\Delta\tilde{T}, \mathrm{CO}_2), \tag{9}$$

where I is a (non-negative) impact indicator, $\mathrm{f}_{\mathbf{p}}(\cdot)$ is the CIRF, $\Delta\tilde{T}$ is the normalized change in GMT compared to

the baseline climate, and CO_2 is the atmospheric CO_2 concentration. The index **p** represents additional parameters that may be varied in the course of a sensitivity analysis.

An inverse analysis involves the translation of an *impact constraint* $I \leqslant I_{\max}$ into the corresponding *climate window*

$$\mathrm{f}_{\mathbf{p}}^{-1}\big([0 : I_{\max}]\big) \equiv \big\{(\Delta\tilde{T}, \mathrm{CO}_2) \,\big|\, \mathrm{f}_{\mathbf{p}}(\Delta\tilde{T}, \mathrm{CO}_2) \leqslant I_{\max}\big\}. \tag{10}$$

For a continuous CIRF, the climate window is fully determined by the *impact isoline*

$$\mathrm{f}_{\mathbf{p}}^{-1}(I_{\max}) \equiv \big\{(\Delta\tilde{T}, \mathrm{CO}_2) \,\big|\, \mathrm{f}_{\mathbf{p}}(\Delta\tilde{T}, \mathrm{CO}_2) = I_{\max}\big\}. \tag{11}$$

The CIRFs presented in this paper were computed for 21 values of ΔT up to $1.6 \times \Delta T_{2\times\mathrm{CO}_2}$, and for 18 levels of CO_2 between 325 and 1000 ppmv. Each function value at one of those sampling points represents the aggregated outcome of a global vegetation simulation on the 0.5° by 0.5° grid. The specified domain of the CIRFs is sufficiently large as to include the time trajectories of the four SRES marker emission scenarios [56] up to the year 2100. The CIRFs themselves do, however, not depend on a particular emission scenario.

2.5. Sensitivity analyses

Climate change and its impacts are still subject to significant uncertainty. We evaluate the sensitivity of the simulated vegetation impacts to the following factors.

Spatial aggregation of the impact indicator

We present both globally averaged and regionally explicit results in this paper. The grid-based simulation of potential vegetation by the BIOME model allows to aggregate impacts up to virtually any world region. As default regionalization, we use the biogeographic regions (syn. floral kingdoms) of the world [68]. While biomes are defined with respect to the *functional* properties of the vegetation, for instance, a similar guild structure, biogeographic regions represent clusters with respect to their *taxonomic* characteristics. Since most concepts of biodiversity are based on taxonomic entities (i.e., species, genera, etc.), we regard it worthy to investigate clusters of them seperately.

Figure 2 provides basic information on the biogeographic regions of the world. Although Capensis covers only parts of the Republic of South Africa, this region is consistently distinguished from Aethiopis due to the high degree of endemism in its flora. Its small size, however, makes Capensis particularly sensitive to the effects of arbitrary local fluctuations in GCM integrations. This scale mismatch lets us abstain from a separate assessment of vegetation impacts in Capensis. Greenland and Antarctis are precluded from the analysis since they are predominantly covered by ice.

Spatial coverage of the impact assessment

In the default case, we focus the impact assessment on protected areas. This is achieved by weighting the simulation results for each grid cell with the extent of protected

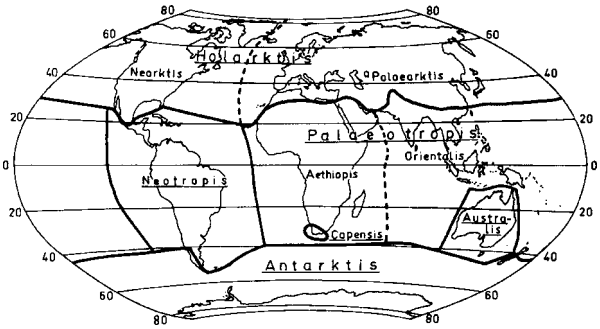

Region	Land area [1000 km^2]	Protected area [%]	Agricultural area [%]
Palaearctis	41580	3.5	20.3
Aethiopis	31550	6.6	5.4
Neotropis	19946	7.5	9.3
Neartctis	18645	6.2	16.5
Orientalis	8081	4.9	41.4
Australis	7464	4.4	4.7
Capensis	1208	2.0	12.4
Antarctis		*not considered here*	
World	128475	5.4	14.7

Figure 2. Biogeographic regions of the world. (Source: [68]; adopted with kind permission from Urban & Fischer.)

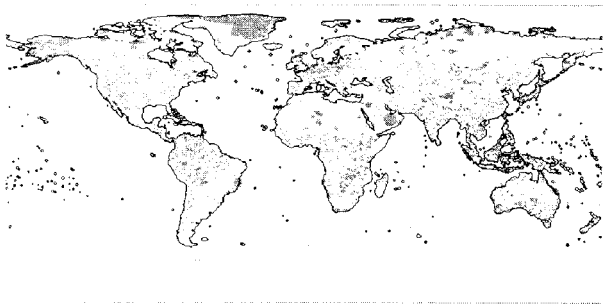

Figure 3. Locations of protected areas. (Source: World Conservation Monitoring Centre [69].)

areas therein according to the most recent version of the *UN List of Protected Areas* [69] (see figure 3). Criteria for the inclusion of a protected area in this list are its size (at least 10 km^2), its management objective (IUCN Categories I to V), and the authority of the management agency (country or federal state level). Alternatively, the total land area and the non-agricultural area [70] of a grid cell are used as weighting factors.

Temporal resolution of the climate change patterns

In the default case, *monthly* climate change patterns for near-surface temperature, precipitation and cloud cover are superimposed onto the baseline climatology. Alternatively, we evaluate the impacts for *annually* averaged climate anomalies.

Source of the climate change projections

Climate change projections from three different GCMs are used for the assessment of climate impacts on the distribution of natural vegetation.

Table 1
Simulated climate impacts on natural vegetation relative to the baseline period (1961–90) for the SRES A1 marker scenario. The climate data refers to changes in annual near-surface temperature (ΔTMP), precipitation (ΔPRC), and cloud cover (ΔCLD).

	ECHAM3 (annual anomalies)		ECHAM3 (monthly anomalies)		ECHAM4 (monthly anomalies)		HadCM2 (monthly anomalies)	
Equilibrium lclimate change for a doubling of the equivalent CO_2 concentration								
$\Delta T_{2\times CO_2}$ (global)	2.69 K		2.69 K		2.79 K		2.78 K	
ΔTMP (land area)	3.70 K		3.70 K		4.39 K		3.94 K	
ΔPRC (land area)	+8%		+8%		+6%		+4%	
ΔCLD (land area)	−2%		−2%		+1%		−1%	
Biome change simulated for the climate of the year 2100[†] (left: total land area; *right: protected areas*)								
Global average	39.1%	*39.1%*	38.4%	*37.1%*	38.7%	*39.0%*	35.1%	*33.9%*
Maximum change in a region	52.7% Nearctis	*60.8% Nearctis*	50.8% Nearctis	*57.3% Palaearctis*	52.0% Nearctis	*65.3% Nearctis*	53.7% Nearctis	*62.3% Nearctis*
Minimum change in a region	28.9% Aethiopis	*23.5% Neotropis*	27.6% Aethiopis	*22.7% Neotropis*	20.7% Australis	*12.7% Australis*	19.2% Aethiopis	*14.9% Aethiopis*
Decade when *global* guard-rail for biome change is exceeded								
10% change	2010s	*2010s*	2010s	*2010s*	2010s	*2010s*	2010s	*2020s*
20% change	2030s	*2030s*	2030s	*2040s*	2030s	*2040s*	2040s	*2040s*
30% change	2060s	*2060s*	2060s	*2060s*	2060s	*2060s*	2070s	*2070s*
Decade when *regional* guard-rail for biome change is exceeded								
20% change	2030s Australis	*2020s Palaearctis*	2030s Palaearctis	*2020s Palaearctis*	2020s Palaearctis	*2020s Palaearctis*	2030s Nearctis	*2030s Palaearctis*
50% change	2090s Nearctis	*2070s Nearctis*	2090s Nearctis	*2070s Palaearctis*	2090s Nearctis	*2060s Palaearctis*	2080s Nearctis	*2070s Nearctis*

[†]For the SRES A1 marker scenario, we calculated $\Delta\bar{T}(2100) = 1.00$ and $CO_2(2100) = 690$ ppmv. The amount of climate change in the year 2100 thus corresponds to the figures stated above for a doubling of the equivalent CO_2 concentration.

3. Results

In this section, we present the main results of our modelling exercise. We first describe the simulated impacts of climate change on natural vegetation for the default settings, both in the forward ('scenario') and inverse ('guard-rail') mode. Subsequently, we present the implications of various sensitivity tests for the CIRFs and the admissible climate windows derived from them.

In the text, we will mostly deal with qualitative aspects of the results whereas quantitative results are presented by means of various impact diagrams. Three types of impact diagrams are used to visualize different aspects of the simulated vegetation impacts, namely biome balance diagrams, response surface diagrams, and impact isoline diagrams. A detailed explanation upon their first use will guide the reader through the diagrams. Due to space limitations, not all qualitative results mentioned in the text can be supported by corresponding impact diagrams.

3.1. Results for specific climate scenarios

Table 1 presents characteristic features of the climate projections from three different GCMs for the SRES A1 marker emission scenario as well as the respective vegetation impacts. The results for the *global* extent of biome change between the baseline climate and the climate of the year 2100 are robust across GCMs, and they correspond well for the total land area and for protected areas. Another robust feature in all simulations is that high-latitude regions (i.e., Nearctis and Palaearctis) are highly sensitive whereas low-latitude regions (e.g., Aethiopis) are comparatively insensitive. Regional variations in the sensitivity of the vegetation are consistently more pronounced for protected areas than for the total land area.

Figure 4 depicts changes in the global extent of biomes between the baseline period and a future point in time in the form of a biome balance diagram. The climate for the year 2100 of the SRES A1 marker scenario is determined by (monthly) climate anomalies from three different GCM experiments. For each biome, the potential area in the baseline climate, the stable area (lower bar), and the total area (upper bar) in equilibrium with the future climate are presented. The difference between the two latter values denotes the newly suitable area of a biome.

The simulated responses differ widely between biomes. The extent of tropical woodland, for instance, almost doubles after complete adaptation to the changed climate, tropical evergreen forest remains largely unaffected, and tundra is predicted to lose about two-thirds of its present area without significant gains elsewhere. Cool conifer forest shows an ambiguous response. Its potential area increases considerably, yet none of the *present* locations of this biome is simulated to remain climatically suitable in 2100.

The simulations for the ECHAM4 and HadCM2 patterns yield more cool mixed forest and hot desert, but less steppe and tropical evergreen forest than for ECHAM3. The differences are moderate and, with the exception of tropical

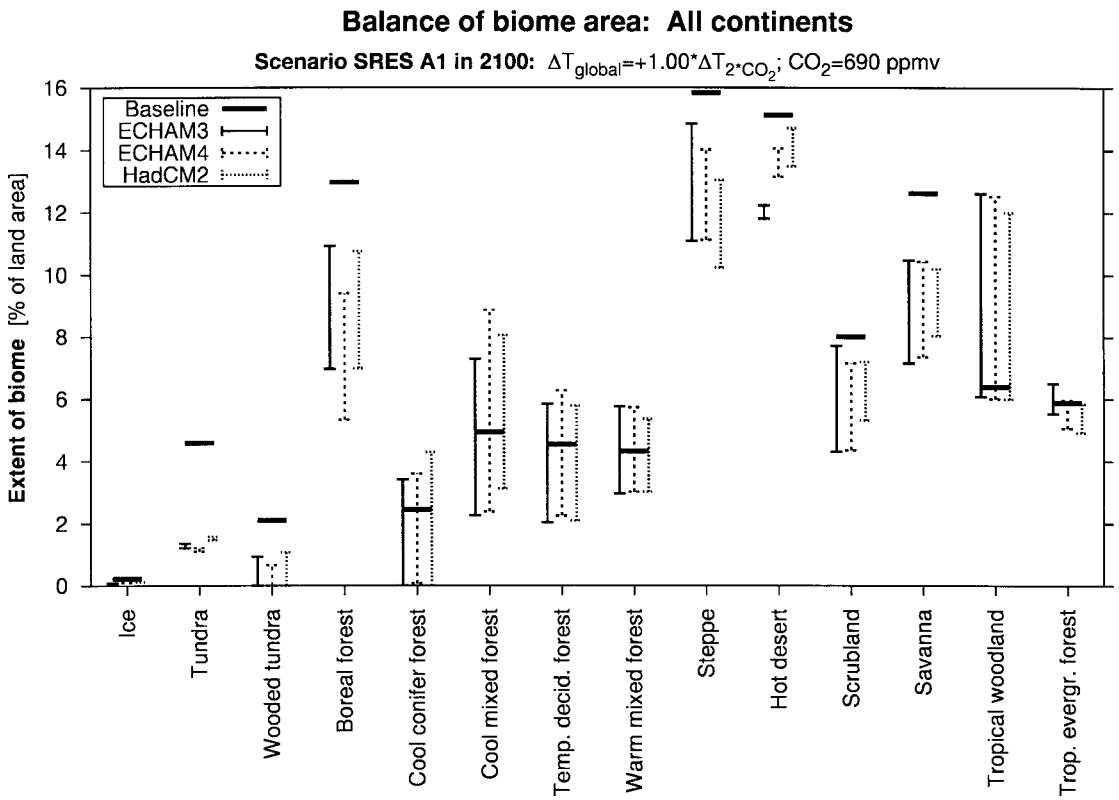

Figure 4. Biome balance diagram for globally averaged changes in potential vegetation between the baseline climate and the climate state simulated by three GCMs for the year 2100 of the SRES A1 marker scenario. ⊥: stable area resp. ⊤: total area of each biome in equilibrium with the *changed* climate.

evergreen forest, there is an agreement on the sign of the projected changes in the total area of each biome.

Whereas biome balance diagrams provide detailed information on the simulated vegetation impacts for *one* future climate state, they are not suitable for inverse analyses of climate change impacts. For this purpose, we developed two alternative diagram types that will be presented in the following section.

3.2. Scenario-independent results

Figure 5 shows the globally averaged response of vegetation in protected areas to changes in GMT and atmospheric CO_2 in a scenario-independent form.

The response surface diagram in figure 5(a) depicts the dose–effect relationship between the two input variables of the CIRF (on the horizontal axes) and the chosen impact indicator (on the vertical axis). The baseline climate is represented by the bottom left corner of the RSD. In geographical terms, the diagram corresponds to a landscape model that states the 'height' of an impact for every 'location' in the climate domain. On the global scale, the relationship between each input factor and the impact indicator is monotonously increasing and rather smooth. The combined effect of changes in both forcing variables is generally larger than the effect of each input factor but less than additive. The coloured isolines connect points on the response surface for which the simulted impacts are equal. In the present example, they correspond to exemplary impact guard-rails that limit the loss of the current biome to 10%, . . . , 50% of protected areas worldwide. The isolines are drawn both on the response surface itself and on the base surface.

A RSD provides an intuitively understandable picture of a CIRF. Due to their 3-dimensional nature, however, RSDs are not well suited for inverse applications.

The impact isoline diagram (IID) in figure 5(b) shows the projection of isolines from the RSD in figure 5(a) onto the domain of the CIRF. In geographical terms, an IID corresponds to a topographical map with contour lines. Climate change is measured both in terms of the absolute change in GMT (below the diagram) and the normalized change in GMT (above the diagram). We also denote the annual mean values of all considered climate variables within the respective region for the baseline climate and for the endpoint of the climate domain. In order to relate the isolines to potential future climate states, we depict the climate trajectories computed by the IRF climate model for the four SRES marker scenarios and for an additional climate stabilization scenario proposed by the German Advisory Council on Global Change [71]. The trajectories start in the bottom left corner of the diagram which represents the climate of the baseline period 1961–1990. Their evolution is denoted in decadal steps until 2100. The '30% guard-rail' is, for instance, violated by the SRES A1 scenario around 2070.

An IID provides a condensed picture of a CIRF in a 2-dimensional diagram. Since IIDs enable the immediate translation of impact constraints into corresponding climate windows, they are particularly suitable for inverse analyses.

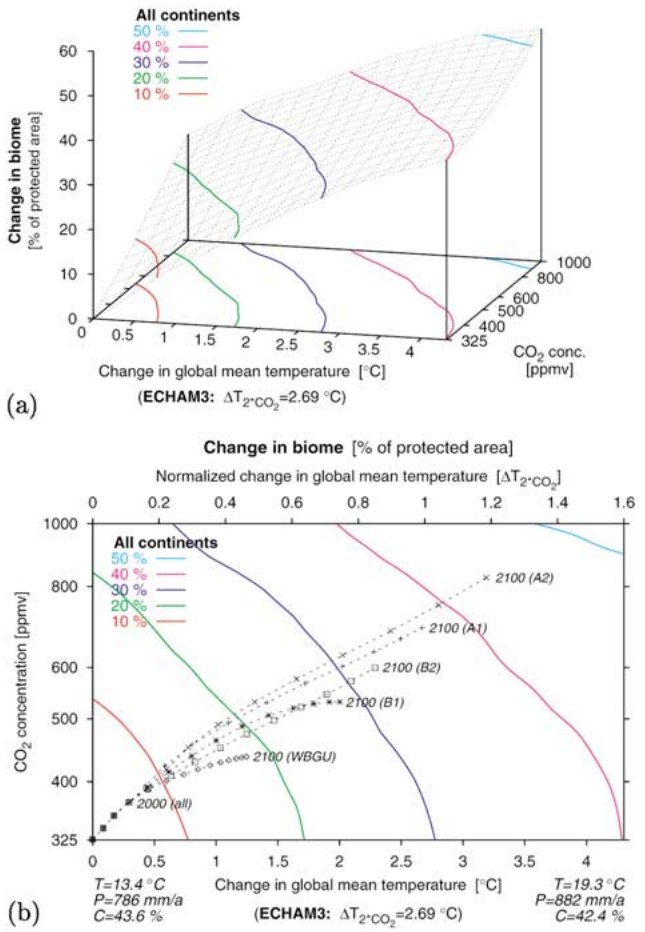

Figure 5. Impact diagrams depicting the percentage of the world's protected areas where the current biome is no longer viable for a range of changes in climate (scaled by the change in global mean temperature) and CO_2 concentration. (a) Response surface diagram. (b) Impact isoline diagram. The climate states reached during the SRES marker scenarios and an additional climate stabilization scenario are depicted in decadal steps from 1970 (bottom left corner) to 2100.

3.3. Regionally specific results

The genetic pools of different biogeographic regions are quite distinct. Merely imposing constraints on globally averaged vegetation impacts is thus likely to be insufficient for the preservation of biodiversity. Therefore, we also determined climate windows based on constraints for regional vegetation change. Selected results are presented in figures 6 and 7.

Figure 6 shows the climate windows for an exemplary impact guard-rail (20% change) in each biogeographic region (coloured isolines) and on the global level (dashed isoline). In high–latitude regions (i.e., Nearctis and Palaearctis), the extent of biome change is typically above the global average (cf. also table 1), and the changing climate is the dominant driver. Biome change in protected areas of Nearctis, for instance, amounts to 50–60% for the changes in *climate* projected for the year 2100 of the SRES A1 marker scenario, and to less than 10% for the respective CO_2 change (figure 7(a)). CO_2 increase is an important driver for vegetation

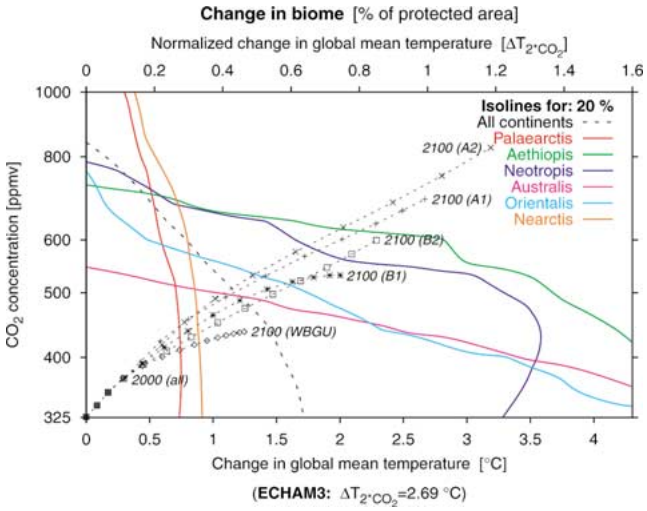

Figure 6. Isoline diagram for biome change in each biogeographic region and on the global level. The guard-rail refers to a change in 20% of the protected area in the respective region.

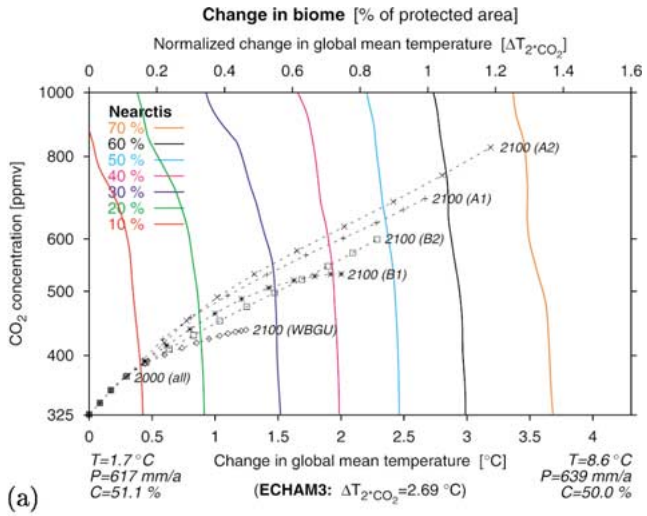

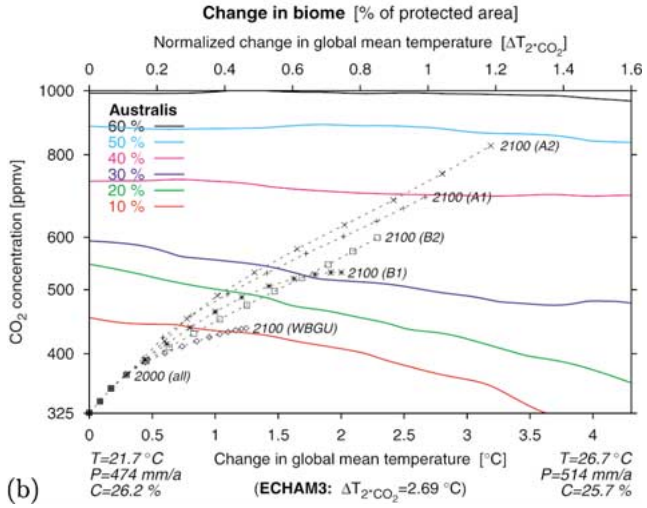

Figure 7. Isoline diagrams for biome change in protected areas of (a) Nearctis and (b) Australis.

change in water-limited regions though. Biome change in protected areas of Australis for the same scenario amounts to 30–40% for changes in CO_2, and to less than 10% for the respective climate change (figure 7(b)). Because of the considerable regional differences in the sensitivity of the vegetation, climate windows become much more restrictive if the impact constraint refers to each region individually instead of the global average.

3.4. Results for individual biomes

It was already shown in figure 4 that the simulated vegetation responses to changes in climate and CO_2 concentration differ widely across biomes. Figure 8 presents climate windows for a 20% decrease in the stable area (figure 8(a)) and the total area (figure 8(b)) of each biome, respectively. Only those biomes are shown where this guard-rail is exceeded within the domain of the CIRF. Predominantly temperature-limited biomes (like wooded tundra, cool conifer forest and tundra) are almost exclusively sensitive to changes in climate variables. These biomes are also the most sensitive ones to climatic changes across all GCM projections. Water-limited biomes (like savanna, scrubland and hot desert) respond strongly to CO_2 changes. The lowest sensitivity to climatic changes is simulated for tropical woodland and tropical evergreen forest.

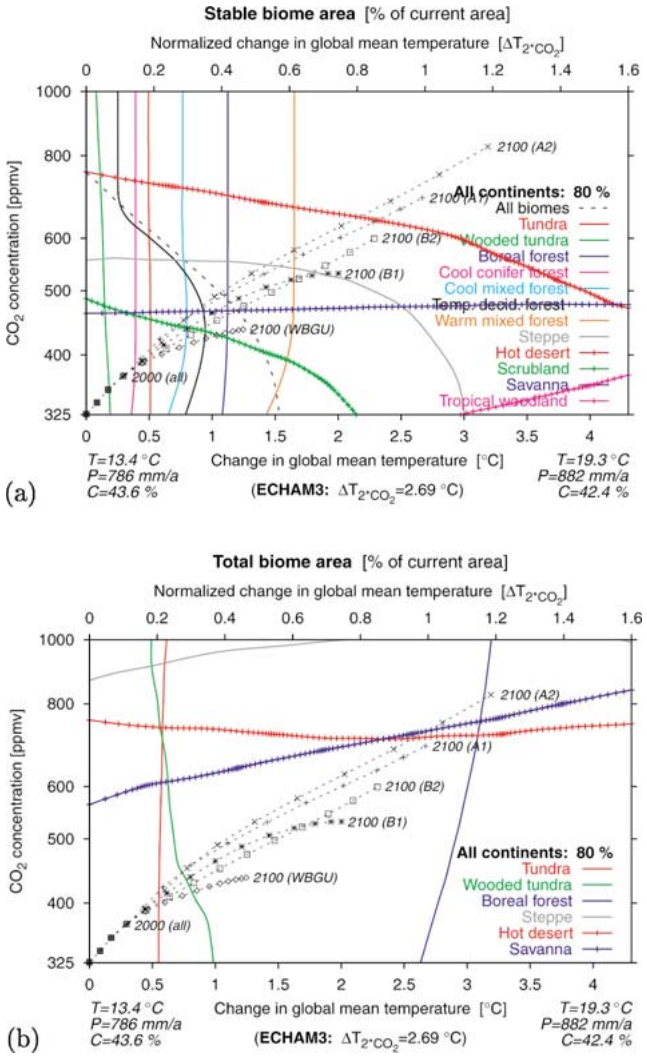

Figure 8. Isoline diagrams for individual biomes. The guard-rail refers to a 20% decrease in the global potential area of each biome (a) *without* and (b) *with* accounting for newly suitable regions.

3.5. Sensitivity to the spatial coverage of the impact assessment

We simulated all vegetation impacts for the protected area, the non-agricultural land area and the total land area in a region. At the global level, there is no significant difference in the results for any of the GCM projections (see table 1). The picture changes somewhat at the level of individual biogeographic regions. On the one hand, protected areas in Orientalis and Neotropis are simulated to be less sensitive to changes in climate and CO_2 concentration than the total land area for three respectively two out of three GCM projections. On the other hand, Nearctis and Palaearctis show more pronounced vegetation changes in protected areas than on average for all GCM patterns. This observation can be explained by the spatial distribution of protected areas within the respective biogeographic regions.

3.6. Sensitivity to the temporal resolution of the climate change patterns

In most regions, simulated vegetation impacts were broadly comparable for monthly and for annually averaged climate change patterns from ECHAM3. The most noticeable exception concerns Australis where vegetation change is less pronounced for seasonally explicit climate anomalies than for annually averaged ones. The major climatic stress for the vegetation in most parts of Australis is low water availability in summer. Since the simulated warming is lowest and the precipitation increase is strongest in that season, scrubland remains suitable after the imposition of seasonally explicit climate anomalies in some regions where it is replaced by the more drought–tolerant steppe after the imposition of annually averaged climate anomalies.

A similar seasonal signal of climate change, essentially characterized by a stronger warming in winter, causes opposite results in Palaearctis. Because vegetation productivity in Palaearctis is predominantly limited by low winter temperatures, seasonally explicit climate anomalies induce more widespread vegetation changes than annually averaged ones.

3.7. Sensitivity to the source of the climate change projection

Figure 9 depicts characteristic IIDs based on climate change patterns from ECHAM4 and HadCM2. In general, the simulated vegetation impacts differ less between ECHAM4 and HadCM2 than between ECHAM3 and either of the other GCMs.

Figure 9(a) shows that global vegetation responds significantly stronger to climate change projections from ECHAM4

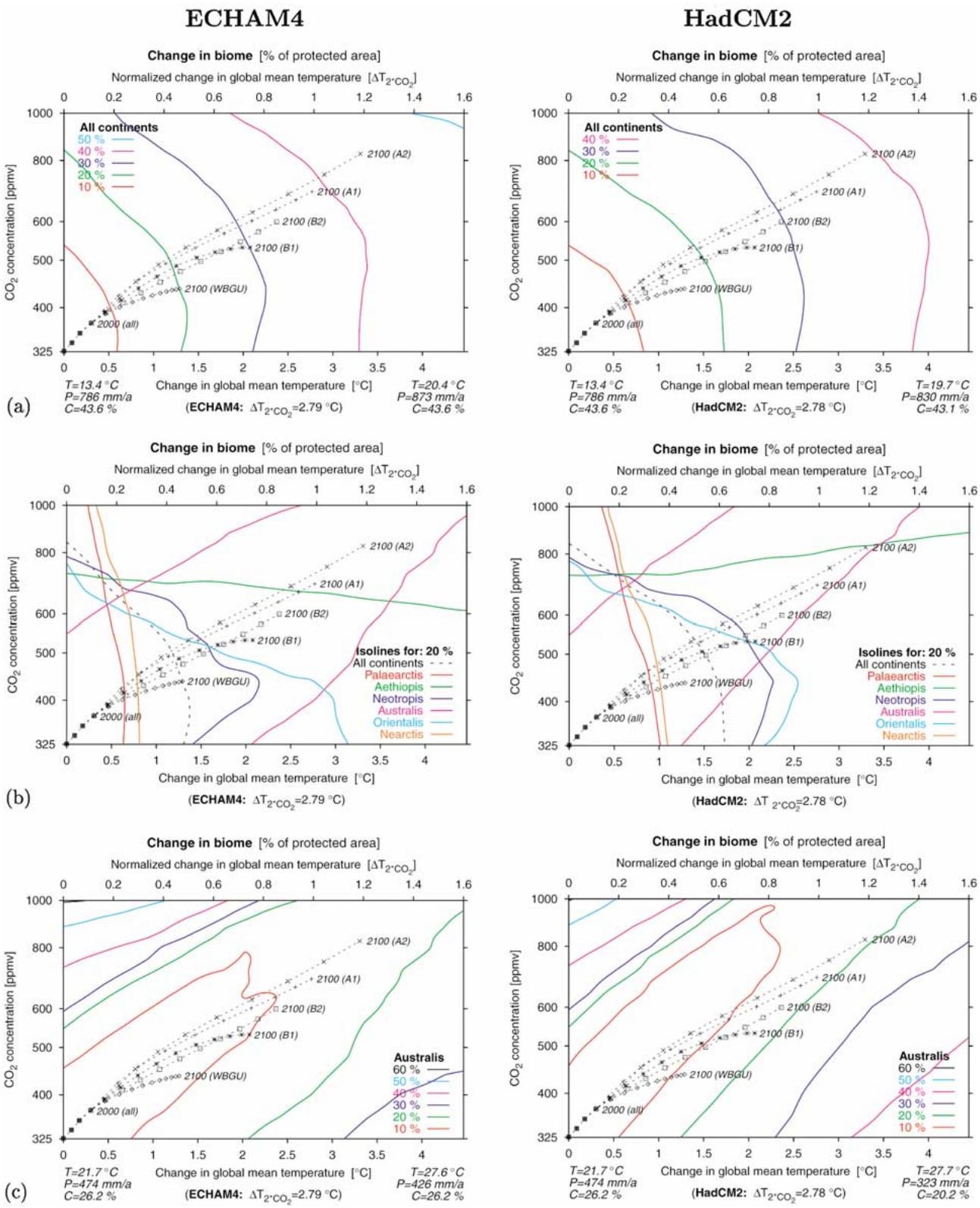

Figure 9. Characteristic vegetation impacts for climate change patterns from ECHAM4 (left) and HadCM2 (right). For a legend and comparable results based on ECHAM3 patterns, see (a) figure 5(b), (b) figure 6, and (c) figure 7(b).

and HadCM2 than to those from ECHAM3 (figure 5(b)) for constant CO_2 concentrations. This observation can be partly explained by the slightly lower continental warming simulated by the latter GCM (see table 1). For more plausible scenarios, comprising changes in both climate and CO_2 concentration, the differences are rather small.

Figure 9(b) depicts impact isolines for all biogeographic regions. Compared to ECHAM3 (figure 6), vegetation responds more sensitive to climate anomalies from ECHAM4 and HadCM2 in Neotropis and Orientalis, and less sensitive in Australis and Aethiopis. In Palaearctis and Nearctis, vegetation impacts based on climate projections from ECHAM3 and ECHAM4 agree well whereas the response is weaker for the HadCM2 projections.

Disagreement between different GCM projections is strongest for Australis. The main reason are large uncertainties in the precipitation projection for this region. The higher water-use efficiency of plants associated with enhanced CO_2 levels partly compensates for the effects of decreasing precipitation as simulated by ECHAM4 and HadCM2. Vegetation impacts throughout the SRES marker scenarios for *combined* changes in climate and CO_2 are therefore smaller than those of changes in climate or CO_2 *alone* (figure 9(b)). Such a compensation effect does not occur for ECHAM3 (figure 7(b)) which projects an increase in precipitation.

4. Summary and conclusions

In this paper, we introduced climate impact response functions (CIRFs) as a convenient method for summarizing and visualizing the impacts of climate-sensitive sectors to changes in fundamental climatic, and possibly other, drivers. CIRFs are particularly suitable for inverse calculations, i.e., for translating impact guard-rails into 'tolerable' climate windows. Furthermore, CIRFs can be applied for assessing regional sensitivities to climatic changes, and to compare the importance of different input factors. In the ICLIPS model, an integrated assessment model of climate change (IAM) based on the guard-rail approach, CIRFs allow the normative specification of minimum requirements for climate protection strategies with respect to the actual impacts of climate change instead of crude proxy variables, like the change in global mean temperature.

We demonstrated the feasibility of the method by assessing the response of natural vegetation to changes in climate and atmospheric CO_2 concentration. The respective impact indicators include the percentage loss of current protected areas and the fractional loss of individual biomes. The latter was evaluated with and without accounting for newly suitable locations. Since we focussed our assessment on areas that are legally protected in their present state, processes like land-use change and the migration of ecosystems were of minor relevance here. Considering the limitations of an intertemporally optimizing global IAM such as the ICLIPS model, we regard these indicators as both comprehensible and relevant to stakeholders.

The BIOME 1 model, as adapted for IMAGE 2.1 to include the effects of enhanced CO_2 levels, was used to simulate the potential vegetation distribution under current and changed climate conditions. BIOME 1 simulates long-term changes in the global vegetation distribution that are in good agreement with more complex dynamic vegetation models, and it is computationally efficient.

Limits for vegetation impacts were translated into corresponding climate windows that are specified in terms of the change in global mean temperature and atmospheric CO_2. Spatial and seasonal variations in the climate change signal as simulated by transient GCM experiments were consistently taken into account by using a scaled scenario approach.

The most extensive vegetation changes were simulated for the high-latitude biomes wooded tundra, cool conifer forest, and tundra where low temperatures are the prime limiting factor for vegetation growth. The distribution of water-restricted biomes like savanna and scrubland was more strongly affected by increasing CO_2 due to its effect on the water-use efficiency of plants. Current areas of tropical woodland and tropical evergreen forest responded least sensitive to anticipated climatic changes. In regions with significant precipitation decreases, the effects of changes in climate and CO_2 were simulated to partly compensate.

We also evaluated the relevance of various assumptions and parameterisations. The vegetation response in protected areas and in the entire land area was comparable at the global level, yet significant differences occurred at the level of biogeographic regions. Simulated impacts for seasonally explicit and annually averaged climate change fields deviated markedly in some regions with a strong seasonal signal in the projected climate anomalies. This argues for climate impact assessments to consider seasonal variations not only in the baseline climatology but also in the climate change signal.

We performed all vegetation simulations for climate projections from three coupled GCMs (ECHAM3, ECHAM4, and HadCM2). These GCM integrations exhibit a comparable climate sensitivity yet their climate change patterns differ considerably. While the vegetation impacts across GCMs agreed well at the global level, significant variations were simulated for some regions. The disagreement was strongest in predominantly water-limited, subtropical regions because variations across GCM projections were greater for precipitation than for temperature.

Certain limitations of the present research exist. Firstly, BIOME 1 neither simulates the vegetation dynamics under the influence of transient climate change and major disturbances, nor does it provide quantitative indicators on the productivity and the carbon dynamics of ecosystems. We therefore selected impact indicators that do not rely on such information. The evaluation of dynamic vegetation models for their applicability in inverse-calculation approaches remains an important topic for future research.

Secondly, simulated biome change is a somewhat coarse indicator for the threat to a protected area. On the one hand, there exist protected areas where the local climate conditions

are inadequately described by the global baseline climatology due to its coarse spatial resolution, or where the preservation of potential natural vegetation is not the primary protection goal. On the other hand, many species in regions with high biodiversity have a small niche volume and are thus more sensitive to climatic change than the biome as a whole. Balancing these arguments, we consider the simulated amount of biome change a low estimate for the threat to terrestrial ecosystems by climatic change.

Finally, the current protected areas do not represent an unbiased sample of global ecosystems, and they are not always located in the centres of biodiversity and endemicity. The legal protection of an area in its current state is, nevertheless, the best information available on the valuation of its ecological features by societies.

To summarize, CIRFs are a valuable means for the aggregated representation of global and regional impacts of climate change for a wide range of future scenarios. They are particularly useful in IAMs based on inverse or optimizing approaches, such as the ICLIPS model, where the on-line simulation of climate impacts by sophisticated models is often infeasible due to their high computational demand.

Acknowledgements

The authors thank Georg Hooss and Reinhard Voss of the Max Planck Institute for Meteorology in Hamburg for the provision of the EOF patterns and the corresponding IRF model from the ECHAM3 integrations. The 1961–90 global mean climatology and the climate change fields from the ECHAM4 and HadCM2 experiments have been obtained through the IPCC Data Distribution Centre. Michael Flechsig and Uta Fritsch of the Potsdam Institute for Climate Impact Research helped with the conversion of the global database on protected areas that was obtained from the World Conservation Monitoring Centre.

Ferenc Tóth and Thomas Bruckner of the Potsdam Institute for Climate Impact Research provided valuable comments on an earlier version of this paper. Anonymous referees also contributed to both the content and the clarity of its presentation. All remaining errors are the sole responsibility of the authors.

Financial support to the ICLIPS project has been provided by the German Federal Ministry of Education and Research (BMBF) under project number 01 LK 9605/0. The views presented here are those of the authors and do not necessarily represent the views of other ICLIPS partners or the project funders.

References

[1] J.T. Houghton, L.G. Meira Filho, B.A. Callander, N. Harris, A. Kattenberg and K. Maskell, eds., *Climate Change 1995. The Science of Climate Change*, Contribution of Working Group I to the Second Assessment Report of the Interngovernmental Panel on Climate Change (Cambridge University Press, Cambridge, 1996).

[2] G. Grabherr, M. Gottfried and H. Pauli, Climate effects on mountain plants, Nature 369 (1994) 448.

[3] B.H. Walker and W.L. Steffen, eds., *Global Change and Terrestrial Ecosystems*, IGBP Book Series No. 2 (Cambridge University Press, Cambridge, 1996).

[4] R.B. Myneni, C.C. Keeling, C.J. Tucker, G. Asrar and R.R. Nemani, Increased plant growth in the northern high latitudes from 1981 to 1991, Nature 386 (1997) 698–702.

[5] A. Menzel and P. Fabian, Growing season extended in Europe, Nature 397 (1999) 659.

[6] H.Q.P. Crick and T.H. Sparks, Climate change related to egg-laying trends, Nature 399 (1999) 423–424.

[7] C. Parmesan, N. Ryrholm, C. Stefanescu, J.K. Hill, C.D. Thomas, H. Descimon, B. Huntley, L. Kaila, J. Kullberg, T. Tammaru, W.J. Tennent, J.A. Thomas and M. Warren, Poleward shifts in geographical ranges of butterfly species associated with regional warming, Nature 399 (1999) 579–583.

[8] C.D. Thomas and J.J. Lennon, Birds extend their ranges northwards, Nature 399 (1999) 213.

[9] J.A. Pounds, M.P.L. Fogden and J.H. Campbell, Biological response to climate change on a tropical mountain, Nature 398 (1999) 611–615.

[10] J.C. McElwain, D.J. Beerling and F.I. Woodward, Fossil plants and global warming at the Triassic–Jurassic boundary, Science 285 (1999) 1386–1390.

[11] P.H. Martin, Will forest preserves protect temperate and boreal biodiversity from climate change?, Forest Ecology and Management 85 (1996) 335–341.

[12] A. Haxeltine and C.I. Prentice, BIOME3: An equilibrium terrestrial biosphere model based on ecophysiological constraints, resource availability, and competition among plant functional types, Global Biogeochemical Cycles 10 (1996) 693–709.

[13] P.N. Halpin, Global climate change and natural-area protection: management responses and research directions, Ecological Applications 7 (1996) 828–843.

[14] L. Villers-Ruíz and I. Trejo-Vázquez, Climate change on Mexican forests and natural protected areas, Global Environmental Change 8 (1998) 141–157.

[15] W.L. Steffen, W. Cramer, M. Ploechl and H. Bugmann, Global vegetation models: incorporating transient changes to structure and composition, Journal of Vegetation Science 7 (1996) 321–328.

[16] A.P. Kirilenko and A.M. Solomon, Modeling dynamic vegetation response to rapid climate change using bioclimatic classification, Climatic Change 38 (1998) 15–49.

[17] J.G. van Minnen, R. Leemans and F. Ihle, Defining the importance of including transient ecosystem responses to simulate C-cycle dynamics in a global change model, Global Change Biology 6 (2000) 595–612.

[18] T.M. Smith, R. Leemans and H.H. Shugart, Sensitivity of terrestrial carbon storage to CO_2-induced climate change: Comparison of four scenarios based on general circulation models, Climatic Change 21 (1992) 367–384.

[19] T.M. Smith and H.H. Shugart, The transient response of terrestrial carbon storage to a perturbed climate, Nature 361 (1993) 523–526.

[20] R.P. Neilson, Vegetation redistribution: a possible biosphere source of CO_2 during climatic change, Water, Air, and Soil Pollution 70 (1993) 659–673.

[21] K. Klein Goldewijk, J.G. van Minnen, G.J.J. Kreileman, M. Vloedbeld and R. Leemans, Simulating the carbon flux between the terrestrial environment and the atmosphere, Water, Air, and Soil Pollution 76 (1994) 199–230.

[22] M. Cao and F.I. Woodward, Dynamic responses of terrestrial ecosystem carbon cycling to global climate change, Nature 393 (1998) 249–252.

[23] P.M. Cox, R.A. Betts, C.D. Jones, S.A. Spall and I.J. Totterdell, Acceleration of global warming due to carbon-cycle feedbacks in a coupled climate model, Nature 408 (2000) 184–187.

[24] G. Petschel-Held, H.-J. Schellnhuber, T. Bruckner, F.L. Tóth and K. Hasselmann, The tolerable windows approach: Theoretical and methodological foundations, Climatic Change 41 (1999) 303–331.

[25] United Nations General Assembly, United Nations Framework Convention on Climate Change, United Nations, New York (1992).
[26] F.L. Tóth, T. Bruckner, H.-M. Füssel, M. Leimbach, G. Petschel-Held and H.-J. Schellnhuber, The tolerable windows approach to integrated assessments, in: *Climate Change and Integrated Assessment Models – Bridging the Gaps. Proceedings of the IPCC Asia-Pacific Workshop on Integrated Assessment Models*, CGER-Report CGER-I029-'97, Center for Global Environmental Research, Ibaraki, Japan (1997) pp. 403–430.
[27] F.L. Tóth, M. Leimbach, T. Bruckner and G. Petschel-Held, Tolerable climate windows and emission corridors: New results with the ICLIPS model, in: *Energy Models for Decision Support – New Challenges and Possible Solutions. Proceedings of the Joint FORUM/ETSAP Workshop*, eds. P. Laege and P. Schaumann (IER, University of Stuttgart, Stuttgart, Germany, 1998) pp. 211–232.
[28] T. Bruckner, G. Petschel-Held, F.L. Tóth, H.-M. Füssel, C. Helm, M. Leimbach and H.-J. Schellnhuber, Climate change decision-support and the tolerable windows approach, Environmental Modeling and Assessment 4 (1999) 217–234.
[29] I.C. Prentice, W. Cramer, S.P. Harrison, R. Leemans, R.A. Monserud and A.M. Solomon, A global biome model based on plant physiology and dominance, soil properties and climate, Journal of Biogeography 19 (1992) 117–134.
[30] J. Alcamo, E. Kreileman, M. Krol, R. Leemans, J. Bollen, J. van Minnen, M. Schaeffer, S. Toet and B. de Vries, Global modelling of environmental change: an overview of IMAGE 2.1, in: *Global Change Scenarios of the 21st Century. Results from the IMAGE 2.1 Model*, eds. J. Alcamo, R. Leemans and E. Kreileman (Pergamon, Oxford, 1998) pp. 3–94.
[31] J. Alcamo, G.J.J. Kreileman, M.S. Krol and G. Zuidema, Modeling the global society–biosphere–climate system. Part 1: Model description and testing, Water, Air, and Soil Pollution 76 (1994) 1–35.
[32] A. Markham, Potential impacts of climate change on ecosystems: a review of implications for policymakers and conservation biologists, Climate Research 6 (1996) 179–191.
[33] R. Leemans, W. Cramer and J.G. van Minnen, Prediction of global biome distribution using bioclimatic equilibrium models, in: *Effects of Global Change on Coniferous Forests and Grassland*, eds. J.M. Melillo and A. Breymeyer (Wiley, New York, 1996) pp. 413–450.
[34] D.N. Yates, T.G.F. Kittel and R.F. Cannon, Comparing the correlative Holdridge model to mechanistic biogeographical models for assessing vegetation distribution response to climatic change, Climatic Change 44 (2000) 59–87.
[35] J.A. Foley, I.C. Prentice, N. Ramankutty, S. Levis, D. Pollard, S. Sitch and A. Haxeltine, An integrated biosphere model of land surface processes, terrestrial carbon balance, and vegetation dynamics, Global Biogeochemical Cycles 10 (1996) 603–628.
[36] R.P. Neilson and S.W. Running, Global dynamic vegetation modelling: Coupling biogeochemistry and biogeography models, in: *Global Change and Terrestrial Ecosystems*, eds., B.H. Walker and W.L. Steffen, IGBP Book Series No. 2 (Cambridge University Press, Cambridge, 1996) pp. 451–465.
[37] Y. Pan, J.M. Melillo, A.D. McGuire, D.W. Kicklighter, L.F. Pitelka, K. Hibbard, L.L. Pierce, S.W. Running, D.S. Ojima, W.J. Parton and D.S. Schimel, Modeled responses of terrestrial ecosystems to elevated atmospheric CO_2: a comparison of simulations by the biogeochemistry models of the Vegetation/Ecosystem Modeling and Analysis Project (VEMAP), Oecologia 114 (1998) 389–404.
[38] R. Leemans and R. Hootsmans, Ecosystem vulnerability and climate protection goals, Report No. 481508004, RIVM, Bilthoven, The Netherlands (September 1998).
[39] M.T. Sykes, I.C. Prentice and F. Laarif, Quantifying the impact of global climate change on potential natural vegetation, Climatic Change 41 (1999) 37–52.
[40] B.A. Bazzaz, Tropical forests in a future climate: Changes in biological diversity and impact on the global carbon cycle, Climatic Change 39 (1998) 317–336.
[41] C. Körner, Tropical forests in a CO_2-rich world, Climatic Change 39 (1998) 297–315.
[42] B. Groombridge, ed., *Biodiversity Data Sourcebook*, WCMC Biodiversity Series No. 1 (World Conservation Press, Cambridge, 1994).
[43] D.M. Olson and E. Dinerstein, The global 200: a representation approach to conserving the Earth's most biologically valuable ecoregions, Conservation Biology 12 (1998) 502–515.
[44] D. Viner, Climate change scenarios for impacts assessment, Aspects of Applied Biology 38 (1994) 13–27.
[45] J.F.B. Mitchell, T.C. Johns, M. Eagles, W.J. Ingram and R.A. Davis, Towards the construction of climate change scenarios, Climatic Change 41 (1999) 547–581.
[46] A. Robock, R.P. Turco, M.A. Harwell, T.P. Ackerman, R. Andressen, H.-S. Chang and M.V.K. Sivakumar, Use of GCM output for impact analysis, Climatic Change 23 (1993) 293–335.
[47] J.B. Smith and G.J. Pitts, Regional climate change scenarios for vulnerability and adaptation assessments, Climatic Change 36 (1997) 3–21.
[48] J.G. van Minnen, J. Alcamo and W. Haupt, Deriving and applying response surface diagrams for evaluating climate change impacts on crop production, Climatic Change 46 (2000) 317–338.
[49] S. Rahmstorf, Bifurcations of the Atlantic thermohaline circulation in response to changes in the hydrological cycle, Nature 378 (1995) 145–149.
[50] K. Hasselmann, R. Sausen, E. Maier-Reimer and R. Voss, On the cold start problem in transient simulations with coupled atmosphere–ocean models, Climate Dynamics 9 (1993) 53–61.
[51] R. Voss and U. Mikolajewicz, Long-term climate changes due to increased CO_2 concentration in the coupled atmosphere–ocean general circulation model ECHAM3/LSG, Climate Dynamics 17 (2001) 45–60.
[52] G. Hooss, R. Voss, K. Hasselmann, E. Maier-Reimer and F. Joos, A nonlinear impulse response model of the coupled carbon cycle–ocean–atmosphere–climate system, Report No. 290, Max Planck Institute for Meteorology, Hamburg, Germany (1999).
[53] H. von Storch and A. Navarra, eds., *Analysis of Climate Variability. Applications of Statistical Techniques* (Springer, Berlin, 1995).
[54] J.B. Smith and M. Hulme, Climate change scenarios, in: *Handbook on Methods for Climate Change Impact Assessment and Adaptation Strategies. Version 2.0*, eds., J.F. Feenstra, I. Burton, J.B. Smith and R.S.J. Tol (United Nations Environment Programme, Nairobi, October 1998) chapter 3.
[55] R. Voss, R. Sausen and U. Cubasch, Periodically synchronously coupled integrations with the atmosphere–ocean general circulation model ECHAM3/LSG, Climate Dynamics 14 (1998) 249–266.
[56] N. Nakicenovic and R. Swart, eds., *Emissions Scenarios* (Cambridge University Press, Cambridge, 2000).
[57] A. Bacher, J.M. Oberhuber and E. Roeckner, ENSO dynamics and seasonal cycle in the tropical Pacific as simulated by the ECHAM4/OPYC3 coupled general circulation model, Climate Dynamics 14 (1998) 431–450.
[58] E. Roeckner, K. Arpe, L. Bengtsson, M. Christoph, M. Claussen, L. Dümenil, M. Esch, M. Giorgetta, U. Schlese and U. Schulzweida, The atmospheric general circulation model ECHAM-4: Model description and simulation of present day climate, Report No. 218, Max Planck Institute for Meteorology, Hamburg, Germany (1996).
[59] T.C. Johns, R.E. Carnell, J.F. Crossley, J.M. Gregory, J.F.B. Mitchell, C.A. Senior, S.F.B. Tett and R.A. Wood, The second Hadley Centre coupled ocean–atmosphere GCM: model description, spinup and validation, Climate Dynamics 13 (1997) 103–134.
[60] M. New, M. Hulme and P. Jones, Representing twentieth century space-time climate variability. Part I: Development of a 1961–1990 mean monthly terrestrial climatology, Journal of Climate 12 (1999) 829–856.
[61] M.A. Semenov and J.R. Porter, Climatic variability and the modelling of crop yields, Agricultural and Forest Meteorology 73 (1995) 265–283.

[62] H. von Storch, Inconsistencies at the interface of climate impact studies and global climate research, Meteorologische Zeitschrift 4 (1995) 72–80.
[63] C.J. Willmott and K. Matsuura, Smart interpolation of annually averaged air temperature in the United States, Journal of Applied Meteorology 34 (1995) 2577–2586.
[64] T.R. Carter, M.L. Parry, H. Harasawa and S. Nishioka, IPCC technical guidelines for assessing climate change impacts and adaptations, Part of the IPCC Special Report to the First Session of the Conference of the Parties to the UN Framework Convention on Climate Change, Department of Geography, University College London, London, UK (1994).
[65] F.L. Toth, W. Cramer and E. Hizsnyik, Climate impact response functions: an introduction, Climatic Change 46 (2000) 225–246.
[66] R. Mendelsohn, M. Schlesinger and L. Williams, Comparing impacts across climate models, Integrated Assessment 1 (2000) 37–48.
[67] T.H. Jones, L.J. Thompson, J.H. Lawton, T.M. Bezemer, R.D. Bardgett, T.M. Blackburn, K.D. Bruce, P.F. Cannon, G.S. Hall, S.E. Hartley, G.Howson, C.G. Jones, C. Kampichler, E. Kandeler and D.A. Ritchie, Impacts of rising atmospheric carbon dioxide on model terrestrial ecosystems, Science 280 (1998) 441–443.
[68] H. Bick, ed., *Ökologie* (Gustav Fischer, Stuttgart, 1989).
[69] IUCN, 1997 United Nations List of Protected Areas, World Conservation Union (IUCN), Gland, Switzerland (1998).
[70] N. Ramankutty and J. Foley, Characterizing patterns of global land use: an analysis of global croplands data, Global Biogeochemical Cycles 12 (1998) 667–685.
[71] WBGU, Targets for climate protection 1997, German Advisory Council on Global Change (WBGU), Bremerhaven, Germany (1997).